Available online at www.sciencedirect.com

SciVerse ScienceDirect

Ceramics International 39 (2013) 3519–3532

CERAMICS INTERNATIONAL

www.elsevier.com/locate/ceramint

A comparative study of hydroxyapatites synthesized using various fuels through aqueous and alcohol mediated combustion routes

R. Ramakrishnan[a], P. Wilson[b,*], T. Sivakumar[a,**], I. Jemina[c]

[a]*Catalysis Laboratory, Department of Applied Science and Technology, A.C.Tech, Anna University, Chennai-600025, India*
[b]*Department of Chemistry, Madras Christian College (Autonomous), Tambaram, Chennai-600 059, India*
[c]*Department of Chemistry, Hindustan Institute of Technology and Science, Hindustan University, Padur, Chennai-603 103, India*

Received 21 August 2012; received in revised form 7 October 2012; accepted 8 October 2012
Available online 18 October 2012

Abstract

Nano-sized calcium hydroxyapatite, $[Ca_{10}(PO_4)_6(OH)_2]$ has been synthesized by the sol–gel combustion method using calcium nitrate and di-ammonium hydrogen phosphate as precursors in the aqueous medium. Triethyl phosphite was used as a phosphate precursor for alcohol mediated combustion. The aqueous and alcohol media were employed for the investigation of combustion synthesis in the presence of various fuels such as urea, glycine, alanine, hydrazine and hexamine. The metal-to-fuel ratio in the synthesis was maintained at 1 to facilitate complete combustion and the Ca/P ratio was maintained at 1.67 to aid the stoichiometric formation of hydroxyapatite. The combustion products were calcined at 800 °C for 10 h and were characterized by powder XRD, FT-IR, HR-SEM and HR-TEM techniques. All the five fuels used under the alcohol mediated combustion, resulted in forming phase pure hydroxyapatite; whereas the aqueous mediated combustion method yielded biphasic calcium phosphate containing $Ca_{10}(PO_4)_6(OH)_2$ and β-TCP depending on the nature of the fuel.

Keywords: A. Powders: chemical preparation; B. Electron microscopy; D. Apatite; E. Sol–gel combustion synthesis

1. Introduction

Hydroxyapatite $[Ca_{10}(PO_4)_6(OH)_2]$ (HA) has been one of the most important biomaterial used in biomedical applications due to its bioactivity, biocompatibility, osteoconductivity and non-toxicity. In addition, these synthesized hydroxyapatite materials possess reasonably a good structural and chemical resemblance to the human bone [1–3]. These properties make hydroxyapatite a superior and highly bio-compatible biomaterial for both the hard and soft tissues. Some of its major biomedical applications include its capacity to serve as matrices for drug release control, owing to its potency to adsorb and desorb bioactive molecules, surface coatings for orthopedic and dental implants, and as bioceramics for fragment replacement [4–7].

Various synthetic routes are available for hydroxyapatite preparation, including mechanochemical synthesis [8] and various techniques of wet synthesis chemistry, such as direct precipitation from aqueous solutions[9,10], electrochemical deposition[11], sol–gel methods [12,13], hydrothermal synthesis [14,15], emulsion or micro emulsion routes [16] and surfactant assisted routes [17] have been attempted. The structural properties of synthesized hydroxyapatite; such as crystallinity, morphology and particle size determine its application. Among the other processes reported in the literature, synthesizing hydroxyapatite by the combustion method is one of the most promising techniques, due to its simple way of synthesizing bioceramics of relatively high porosity, and cost effective strategy [18].

Combustion synthesis has been considered as an significant and facile route for of synthesizing and processing advanced transition metal oxides [19,20], catalysts [21,22], composites [23], phosphors [24,25], inter-metallic [26] and

*Corresponding author. Tel.: +91 44 9841426693.
**Corresponding author. Tel.: +91 44 22359193; fax: +91 44 22352642.
E-mail addresses: catwils@gmail.com (P. Wilson), tssivakumar@yahoo.com (T. Sivakumar).

0272-8842/$ - see front matter © 2012 Elsevier Ltd and Techna Group S.r.l. All rights reserved.
http://dx.doi.org/10.1016/j.ceramint.2012.10.176

nanomaterial [27,28]. In addition, propulsion chemistry involves processes that concern thermally induced exothermic redox reactions taking place between the oxidant and fuel, under a suitable reaction temperature. Solution combustion synthesis is an emerging method of producing homogeneous, pure and nano-crystalline materials at low reaction temperatures, and is considered to be a better method than other conventional processes. This method involves combustion by heating the corresponding metal precursors and fuel in a stoichiometric ratio.

Usually nitrates are widely used as oxidizers and organic fuels such as urea [28], glycine [29], hexamethylene tetramine (HMT) [30], asparagine, serine [31], methyl cellulose [32], ammonium acetate, ammonium citrate and ammonium tartarate [33], citric acid [34], tartaric acid [35] amines [36], and hydrazides [18] have already been used in the solution combustion methods. Various transition metal oxides, such as Al_2O_3, SiO_2, CeO_2, ZrO_2, Fe_2O_3, TiO_2, metal doped metal oxides [18], pervoskite oxide materials [37], refractory materials like CaO, and MgO [38], luminescent materials such as rare earth metal doped Y_2O_3 [39] and insulating oxide such as ZnO [40] have already been synthesized using a different variety of fuels.

The basic concept of combustion synthesis involves the thermo-chemical reactions used in the field of propellants and explosives chemistry. During the synthesis of hydroxyapatite, the metal-to-fuel ratio is normally made to be unity, while the Ca^{2+}/PO_4^{3-} ratio is maintained at 1.67. Stoichiometric metal to fuel ratio is an important parameter for facilitating stable combustion and the formation of hydroxyapatite materials with minimum carbon deposits, owing to the maximum heat energy involved in the process. Excess metal (oxidizer)-to-fuel ratio leads an incomplete reaction, resulting in carbon deposits. The major gaseous products of combustion reaction are CO_2, H_2O and N_2. The stoichiometric ratio (M/F) of a metal(M) to fuel(F) mixture can be obtained using the total oxidizing and reducing valences of the reactants, which serve as numerical coefficients for stoichiometric balance and the same can be expressed as follows [41]:

M/F = $\sum$ (coefficients of elements in the molecular formula of the oxidizer salt) x (valency)/ $\sum$ (coefficients of elements in the molecular formula of the fuel) x (valency) where, M = metal nitrates or oxidizer and F = Fuel.

Recently several papers have reported the combustion method for the synthesis of hydroxyapatites for the past two decades. Hydroxyapatites have been synthesized using the polymeric combustion process, using $Ca(NO_3)_2 \cdot 4H_2O$ and triethyl phosphate as precursor [42]; In addition, modified self-propagating combustion synthesis using calcium nitrate, diammonium hydrogen orthophosphate (DAP) as precursors and urea as an organic fuel [43]; by citric acid sol–gel combustion method [44]; employing urea and glycine as fuels [45] have been attempted. Besides, hydroxyapatite nanotubes were also synthesized, using sol–gel auto-combustion method with a porous anodic aluminum oxide (AAO) template [46].

However, there have been only a few reports available on the synthesis of hydroxyapatite via the combustion route [42–46]. Moreover, in particular, the information regarding the influence of employing various fuels on the morphological properties of hydroxyapatite in a given medium during synthesis has not been explored throughout the literature.

In the present sturdy, sol–gel combustion synthesis of hydroxyapatite, have been carried out to investigate, (i) the influence of aqueous and alcohol medium on the hydroxyapatite phase formation, (ii) the nature of combustion by choosing the variety of organic fuels such as glycine, alanine, urea, hydrazine and hexamine (iii) the influence of maintaining stoichiometric composition of metal to fuel ratio and stoichiometric composition of Ca/P to synthesize stoichiometric hydroxyapatite and (iv) employing acidic conditions by adding Conc. nitric acid in both aqueous and alcohol media in preventing carbon deposition during the combustion process due to its oxidizing property.

2. Materials and methods

2.1. Experimental methods

2.1.1. Aqueous mediated sol–gel combustion synthesis of hydroxyapatites

Calcium nitrate, $Ca(NO_3)_2 \cdot 4H_2O$ (Sigma-Aldrich) and di-ammonium hydrogen ortho-phosphate [$(NH_4)_2HPO_4$] (SRL Chemicals) were used as calcium and phosphate precursors for the synthesis of hydroxyapatites. To a stoichiometric amount of calcium nitrate in double distilled water, a calculated amount of aqueous ammonia (SRL Chemicals) was added in drops until the pH of the solution attained 11. After adjusting the pH of the solution, a stoichiometric amount of di-ammonium hydrogen phosphate in double distilled water was added in drops from the burette very slowly (0.5 ml/min) into the beaker while stirring its contents with the magnetic stirrer. Adequate care was taken to maintain the pH of the reaction mixture above 10.5–11. The milky suspension formed, was stirred continuously for about 3 h.

The milky white precipitate was then dissolved by using Conc. nitric acid (Merck) and the pH was dropped to about 1, resulting in the formation of a clear transparent solution. The solution obtained was concentrated by heating it to about 110 °C. Subsequently, a calculated amount of urea (Merck) was added as fuel to the above concentrated solution, and the contents were stirred for about 10 min at room temperature. The white viscous sol thus formed was further combusted in a muffle furnace, normally in the temperature range of 180–450 °C at a rate of about 2 °C/min. After the combustion process was over, the heating was continued to reach 500 °C and the same temperature was maintained for 20 min followed by cooling to room temperature. The sample thus obtained was finely ground, dried at 110 °C for 24 h and calcined at 800 °C for 10 h. Thus, by adopting the above procedure but by

varying the fuels such as glycine, alanine, hexamine and hydrazine hydrate (SRL Chemicals) a number of hydroxyapatites were synthesized. In all the above processes of synthesis, the metal-to-fuel ratio and the Ca/P ratios were maintained at 1:1 and 1.67 respectively. The general flowchart for the process is shown in Fig. 1.

2.1.2. Alcohol mediated sol–gel combustion synthesis of hydroxyapatite

Calcium nitrate, $Ca(NO_3)_2 \cdot 4H_2O$ (Sigma-Aldrich) and triethyl phosphite (Sigma-Aldrich) were used as calcium and phosphate precursors respectively. Triethyl phosphite of the desired molar composition was dissolved in 97 ml of ethanol (Merck); 3 ml of deionized water was added to the solution and stirred for 3 h. The vanishing smell of triethyl phosphite indicates the completion of its hydrolysis. To this solution, a stoichiometric amount calcium nitrate dissolved in double distilled water was added drop wise, (0.5 ml/min) while stirring. After the addition of the phosphate precursor, a clear homogeneous solution was formed; it was stirred for 12 h at room temperature.

The clear solution was concentrated by heating it to about 110 °C, and the given fuel was added to the clear and concentrated solution which led to the formation of the gel. Ethanol insoluble fuels were dissolved in small amounts of water prior to its addition to the sol solution, so as to form the gel. The gel thus obtained was combusted in a muffle furnace heated to 500 °C at a rate of about 2 °C/min. The heating was continued till 500 °C, and the same temperature was maintained for 20 min. Subsequently, the product obtained after the combustion was allowed to cool to room temperature, finely ground, dried at 110 °C for 24 h and calcined at 800 °C for 10 h. Thus, a series of hydroxyapatites were synthesized in the above manner by adopting the above procedure using different fuels such as glycine, alanine, hexamine and hydrazine hydrate, (SRL Chemicals). The metal-to-fuel ratio and the Ca/P ratios were maintained at 1:1 and 1.67 respectively in all the samples, prepared using various fuels. The general flowchart for the process is shown in Fig. 2.

2.1.3. Synthesis of hydroxyapatite by sol–gel method

The sol–gel synthesis of phase pure hydroxyapatite has been reported elsewhere [12,13]. Hydroxyapatite material has also been synthesized in the present investigation through the sol–gel method, for the purpose of comparison by adopting the procedure referred to in the literature. Calcium nitrate, $Ca(NO_3)_2 \cdot 4H_2O$ (Sigma-Aldrich) and di-ammonium hydrogen ortho-phosphate $[(NH_4)_2HPO_4]$ (SRL Chemicals) were used as the calcium and phosphate precursors for the synthesis of hydroxyapatites. A stoichiometric amount of calcium nitrate was dissolved in double distilled water, and a calculated amount of aqueous ammonia (SRL Chemicals) was added in drops to maintain the pH above 11. After adjusting the pH of the solution, a stoichiometric amount of di-ammonium hydrogen phosphate (Ca/P = 1.67) was dissolved in double distilled water and the same was added in drops from the burette at a flow rate of about 0.5 ml/min into the beaker

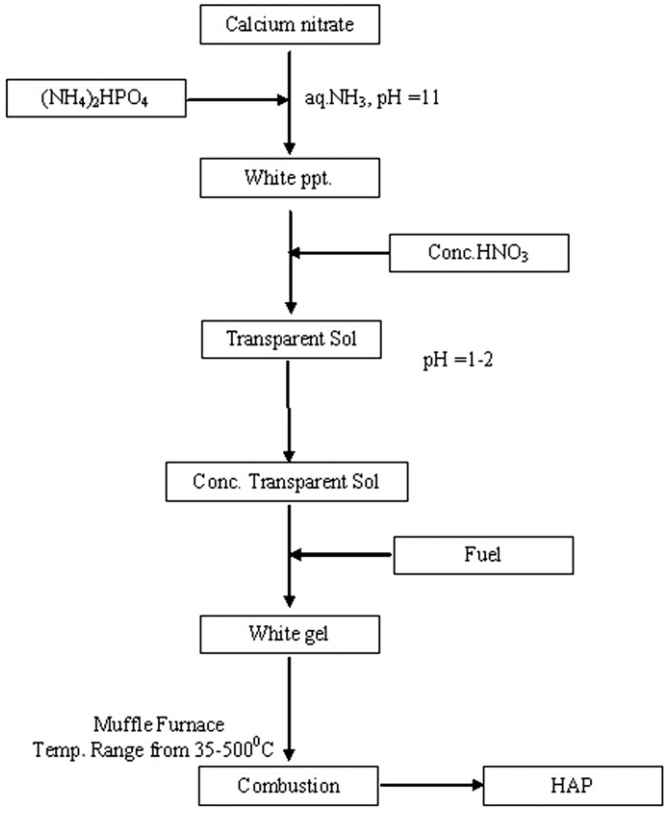

Fig. 1. The typical flow chart representation of hydroxyapatite synthesized by aqueous mediated sol–gel combustion method using various fuels.

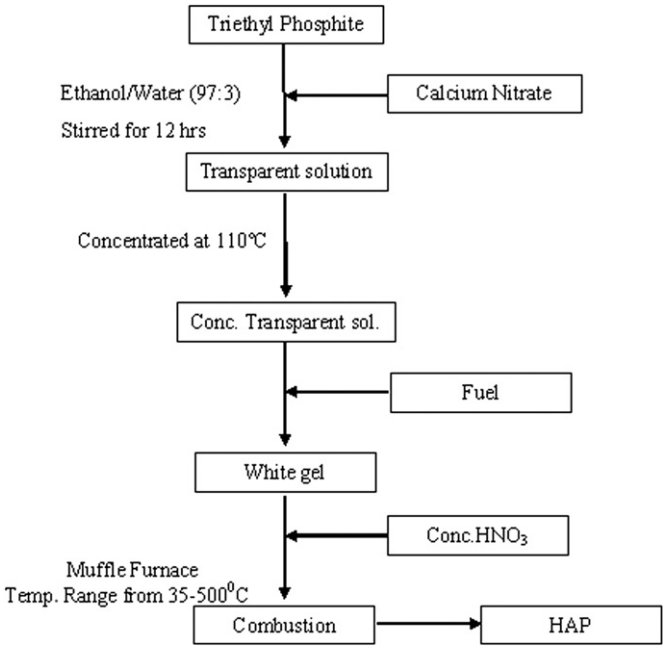

Fig. 2. The typical flow chart flow chart representation of hydroxyapatite synthesized by alcohol mediated sol–gel combustion method using various fuels.

while stirring its contents with magnetic stirrer at room temperature. Adequate care was taken to maintain the pH of the reaction mixture above 10.5–11 by the proper addition of aq. ammonia. The milky suspension was formed, after the continuous addition of phosphate species, and the stirring was continued for about 6 h to ensure that proper mixing takes place. This was followed by ageing for 24 h at room temperature. Subsequently, the precipitate formed was filtered through whatman filter paper, and washed with double distilled water, and dried at 110 °C for 24 h. The samples were then finely ground, and calcined at 800 °C for 10 h, at ambient conditions.

2.2. Characterizations

The phase composition and crystallinity of the calcined samples were analyzed using the powder X-Ray diffraction technique. Guiner powder diffractometer SAIFERT BYZ 2002 MODEL was used for recording the 2 theta values ranging from 20 and 70 deg using Cu K_α ($\lambda = 1.54056$ A°) as a source radiated at 30 kV and 20 mA. The obtained ASCII. data was analyzed using origin 8 software. The peak indexing was done by using standard data from the JCPDF Card no. #09–0423 and other calcium phosphate cards were used for the analysis. The least square method was used to refine the unit cell parameters. Infrared spectra were recorded using Thermo-Nicolet IR 2000 IR spectrometer for determining the various group frequencies and chemical structure for the synthesized and calcined hydroxyapatite samples. The samples were scanned at the frequency range of 4000 to 400 cm^{-1}, by averaging 16 scans at a resolution of 4 cm^{-1}. The particle morphology of the calcined hydroxyapatite powder samples was investigated by using the FEI Quanta FEG 200—High Resolution Scanning Electron Microscope (HR-SEM) operated at 20 kV and 30 kV. The microstructures and morphological features of the alcohol mediated combustion synthesized hydroxyapatites were studied with a High Resolution Transmission Electron Microscope (HR-TEM; JEOL JEM-2100 F), equipped with an energy-dispersive X-ray spectroscopy (EDS, JEOL JXA-840) with an operating voltage of 200 kV.

3. Results

3.1. Powder X-Ray diffraction (PXRD)

The X-Ray powder diffraction patterns for the hydroxyapatites, prepared through both aqueous and alcohol mediated combustion routes and calcined at 800 °C, show that the hydroxyapatites are quite crystalline in nature, as it is evident from the enhanced intensity of the diffraction peaks as shown in Figs. 3 and 4.

The characteristic XRD patterns of the hydroxyapatites synthesized by both aqueous and organic mediated combustion processes are identified and indexed by comparing with the standard JCPDF card no. (09–0432). The

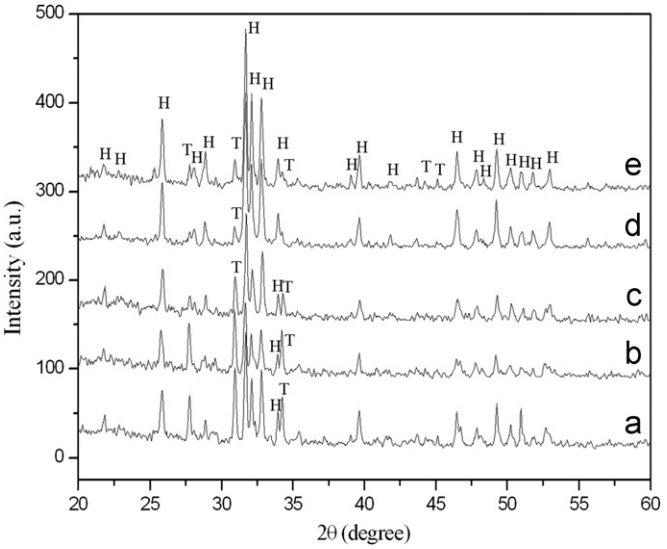

Fig. 3. X-Ray diffraction pattern of aqueous combustion mediated synthesis of hydroxyapatite using various fuels such as glycine, alanine, urea, hydrazine and hexamine. [H-Hydroxyapatite, T-Tricalcium phosphate].

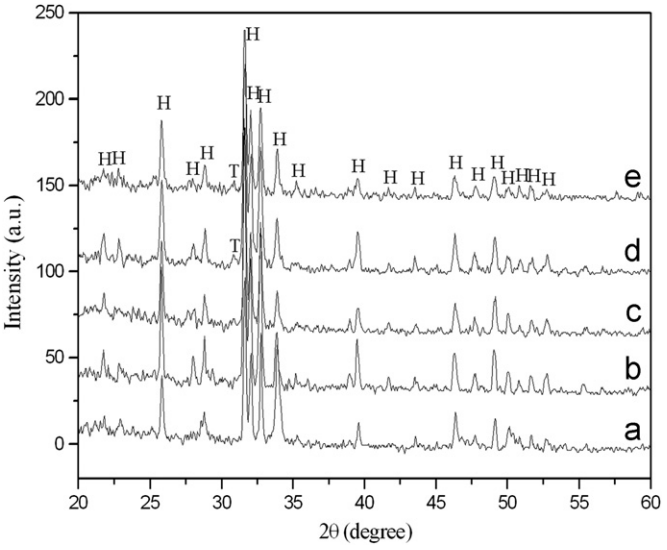

Fig. 4. X-Ray diffraction pattern of alcohol mediated combustion synthesis of hydroxyapatite by using various fuels such as glycine, alanine, urea, hydrazine and hexamine. [H-Hydroxyapatite, T-Tricalcium phosphate].

diffraction patterns at $2\theta = 37.347$, 53.856 (04–0777) and $2\theta = 18.08$, 34.088 (04–0733) are completely absent, suggesting the absence of corresponding CaO and $Ca(OH)_2$ phases.

The peak broadening of the diffraction reflection have been used to estimate the crystallite size in a direction perpendicular to the crystallographic plane based on Scherer's formula as represented:

$$X_S = 0.9\lambda/(\mathrm{FWHM} \times \cos\theta)$$

where X_S—crystallite size (nm), λ—wavelength of the monochromatic x-ray beam (nm), FWHM—Full width at half maximum for the diffraction peak under consideration (rad) and θ–diffraction angle [47].

The presence of tricalcium phosphate (β-TCP) can be identified in the case of an aqueous mediated combustion product, depending on the nature of fuel used. This can be identified by comparing the XRD data with the standard JCPDF card no. 09–0169.

The HAP/TCP phase percentage can be obtained by the relative intensity ratio (RIR) as mentioned elsewhere [48,49]. This can be achieved by comparing the intense peak of the hydroxyapatite and the TCP corresponding to the hkl values of (211) and (0210).

$$\text{Relative Intensity Ratio (RIR)} = I_{\beta-TCP}/(I_{HAP}+I_{\beta-TCP}) \times 100$$

The above ratio indicates the extent of the phase purity of the hydroxyapatite samples, prepared via aqueous and organic mediated combustion methods using various fuels. The RIR parameter for samples synthesized through the organic mediated combustion method was found to be less than 0.3 suggesting the presence of phase pure hydroxyapatites. However, a comparison of the RIR values of the hydroxyapatite obtained via aqueous mediated combustion method, suggests that hydrazine and hexamine have produced a relatively less amount of TCP, when compared with the other fuels, as shown in Table 1.

The fraction of the crystalline phase (X_c) or degree of crystallinity for the hydroxyapatites obtained through the combustion process, calcined at 800 °C for 10 h, can be evaluated from the following equation:

$$X_c = 1-(V_{112/300}/I_{300})$$

where I_{300} is the intensity of (300) diffraction peak and $V_{112/300}$ is the intensity of hollow between (112) and (300) diffraction peak of the hydroxyapatite [50].

The unit cell parameters were indexed using a hexagonal unit cell with the $P6_3/m$ (No.176) and lattice parameters of a=b=9.432 A°, c=6.881 A° and Z=1.The least squared refined lattice parameters, for the hydroxyapatite samples prepared through aqueous and organic mediated routes have been listed in Tables 1 and 2 respectively. The lattice parameters were determined by using the formula [51]:

$$1/d^2 = 4/3[h^2+hk+k^2/a^2]+l^2/c^2$$

The equation employed to obtain the volume of the unit cell is given below:

$$V = a^2c*\sin 60^\circ \text{or} V = \sqrt{3}/2a^2c$$

The calculated values of the average crystallite size (X_s), the fraction of the crystalline phase (X_c), relative intensity ratio (RIR), and the approximate particle diameter calculated from SEM similar to the procedure adopted by S.K.Ghosh et. al. [45], in addition to the lattice parameter for the hydroxyapatite synthesized using aqueous and alcohol mediated synthesis using different fuels are shown in Tables 1–4 respectively.

Table 2
Crystallite size and approximate particle diameter calculated from SEM, for hydroxyapatites synthesized by aqueous medium using different fuels.

Fuel	Avg. crystallite size calculated for miller planes (nm)				Approximate particle diameter (nm)
	0 0 2	3 1 0	2 2 2	2 1 3	
Glycine	34.8	41.4	42.7	39.0	50–400
Alanine	32.5	39.7	37.1	38.0	70–250
Urea	38.0	36.5	39.0	37.8	75–300
Hydrazine	34.0	38.0	34.1	46.0	50–250
Hexamine	47.9	33.7	46.0	46.6	80–300

Table 3
Relative intensity ratio, crystallinity degree and lattice parameter of hydroxyapatites synthesized by alcohol medium using different fuels.

Fuel	Relative intensity ratio (RIR) HAP/TCP	Crystallinity degree (X_c) %	Lattice parameters		
			a (nm)	c (nm)	Volume (A°)^3
Glycine	99.8/0.2	82	0.9462	0.6890	534.2
Alanine	99.9/0.1	68	0.9473	0.6900	536.3
Urea	99.9/0.1	96	0.9470	0.6906	536.4
Hydrazine	99.4/0.3	93	0.9473	0.6890	535.5
Hexamine	99.8/0.2	98	0.9462	0.6902	535.1
Sol–gel*	99.9/0.1	82	0.9420	0.6866	527.7

*Refer 2.1.3. Synthesis of hydroxyapatite by sol–gel method.

Table 1
Relative intensity ratio, crystallinity degree and lattice parameters of hydroxyapatites synthesized by aqueous medium using different fuels.

Fuel	Relative intensity ratio (RIR) HAP/TCP	Crystallinity degree (X_c) %	Lattice parameters		
			a (nm)	c (nm)	volume (A°)^3
Glycine	64/36	84	0.9451	0.6880	532.2
Alanine	53/47	93	0.9451	0.6920	535.3
Urea	72/28	89	0.9430	0.6880	529.8
Hydrazine	90/10	68	0.9460	0.6900	534.8
Hexamine	85/15	98	0.9432	0.6890	530.8
Sol–gel*	99.9/0.1	82	0.9420	0.6866	527.7

*Refer 2.1.3. Synthesis of hydroxyapatite by sol–gel method.

Table 4
Crystallite size and approximate particle diameter calculated from SEM, for hydroxyapatites synthesized by alcohol medium using different fuels.

Fuel	Avg. crystallite size calculated for miller planes (nm)				Approximate particle diameter (nm)
	0 0 2	3 1 0	2 2 2	2 1 3	
Glycine	46.8	51.6	44.1	44.1	90–300
Alanine	42.8	41.7	32.7	41.2	150–500
Urea	49.9	43.4	45.8	35.1	80–300
Hydrazine	36.0	30.8	40.2	32.3	90–290
Hexamine	43.4	32.5	29.3	30.2	90–270

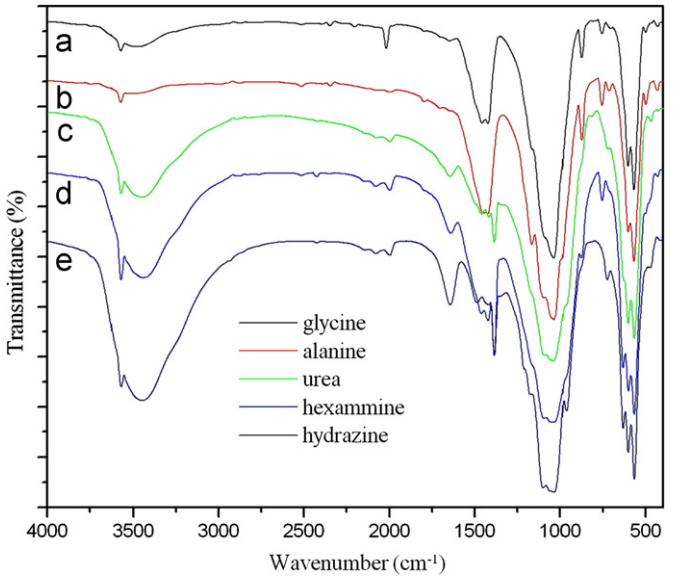

Fig. 5. FT-IR spectrum of hydroxyapatite synthesized by aqueous phase sol–gel combustion method using various fuels such as (a) glycine, (b) alanine, (c) urea, (d) hexamine and (e) hydrazine, dried at 110 °C for 24 h.

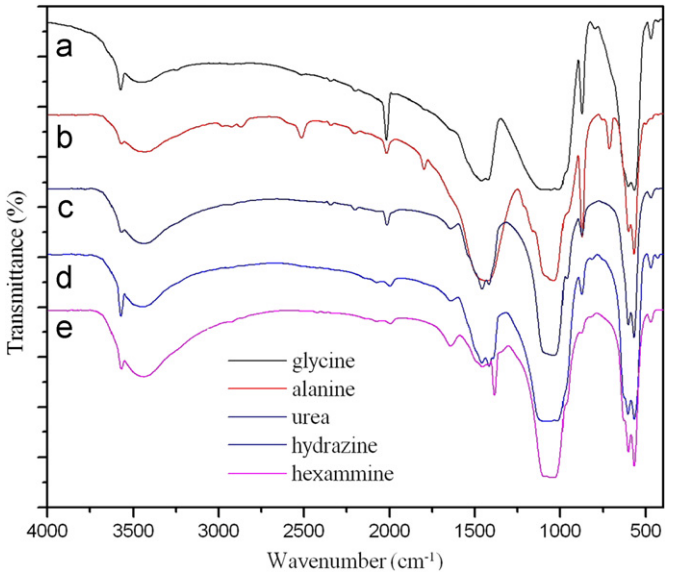

Fig. 6. FT-IR spectrum of hydroxyapatite synthesized by alcohol phase sol–gel combustion method various fuels such as (a) glycine, (b) alanine, (c) urea, (d) hydrazine and (e) hexamine, dried at 110 °C for 24 h.

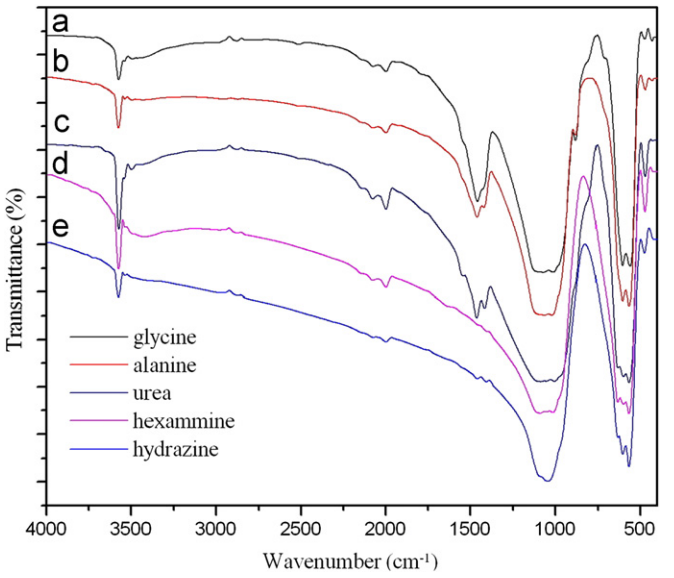

Fig. 7. FT-IR spectrum of hydroxyapatite synthesized by aqueous phase sol–gel combustion method various fuels such as (a).glycine, (b).alanine, (c). urea,(d).hexamine, and (e).hydrazine calcined at 800 °C for 10 h.

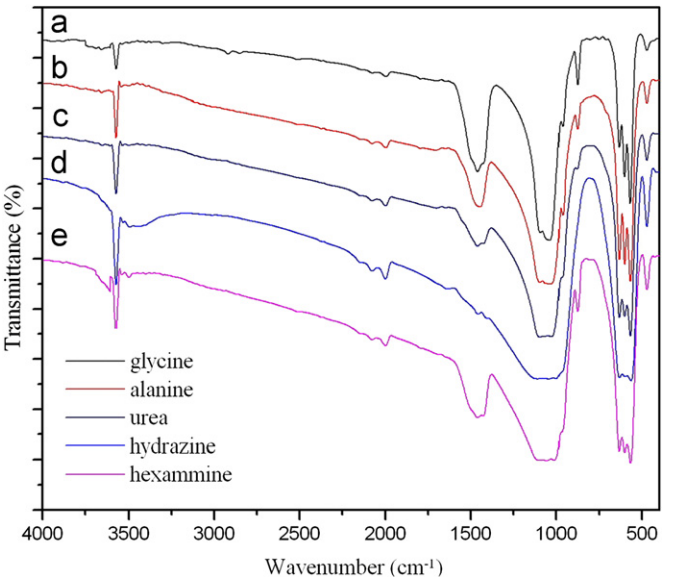

Fig. 8. FT-IR spectrum of hydroxyapatite synthesized by alcohol mediated sol–gel combustion method various fuels such as glycine, alanine, urea, hydrazine and hexamine, calcined at 800 °C for 10 h.

3.2. Fourier transform infrared spectroscopy (FT-IR)

The FT-IR spectra of hydroxyapatites synthesized by both aqueous and alcohol mediated combustion methods and dried at 110 °C for 24 h are shown in Figs. 5 and 6. The broad bands in the wave number range from 3573 cm^{-1} to 2500 cm^{-1}; and a relatively intense peak at 632 cm^{-1} arises from the stretching and vibrational modes of the OH groups. The band at 1635 cm^{-1} is derived from the v_2 bending modes of the H_2O molecules. The band at 3573 cm^{-1} is assigned to the non-hydrogen bonded OH

stretching mode, usually assigned to the hydroxyl group of hydroxyapatite and the band centering at 3447 cm^{-1}, arises due to the hydrogen bonded OH stretching. However, it can be inferred that the water content of the samples prepared through alcohol mediated combustion synthesis is comparatively less. The peaks at 1090 cm^{-1} and about 1034 cm^{-1} band arise due to the triply degenerate v_3 antisymmetric PO stretching mode of PO_4^{3-}. The 963 cm^{-1} band arises from the nondegenerate PO symmetric stretching mode v_1 PO_4^{3-}. The 603 cm^{-1} and

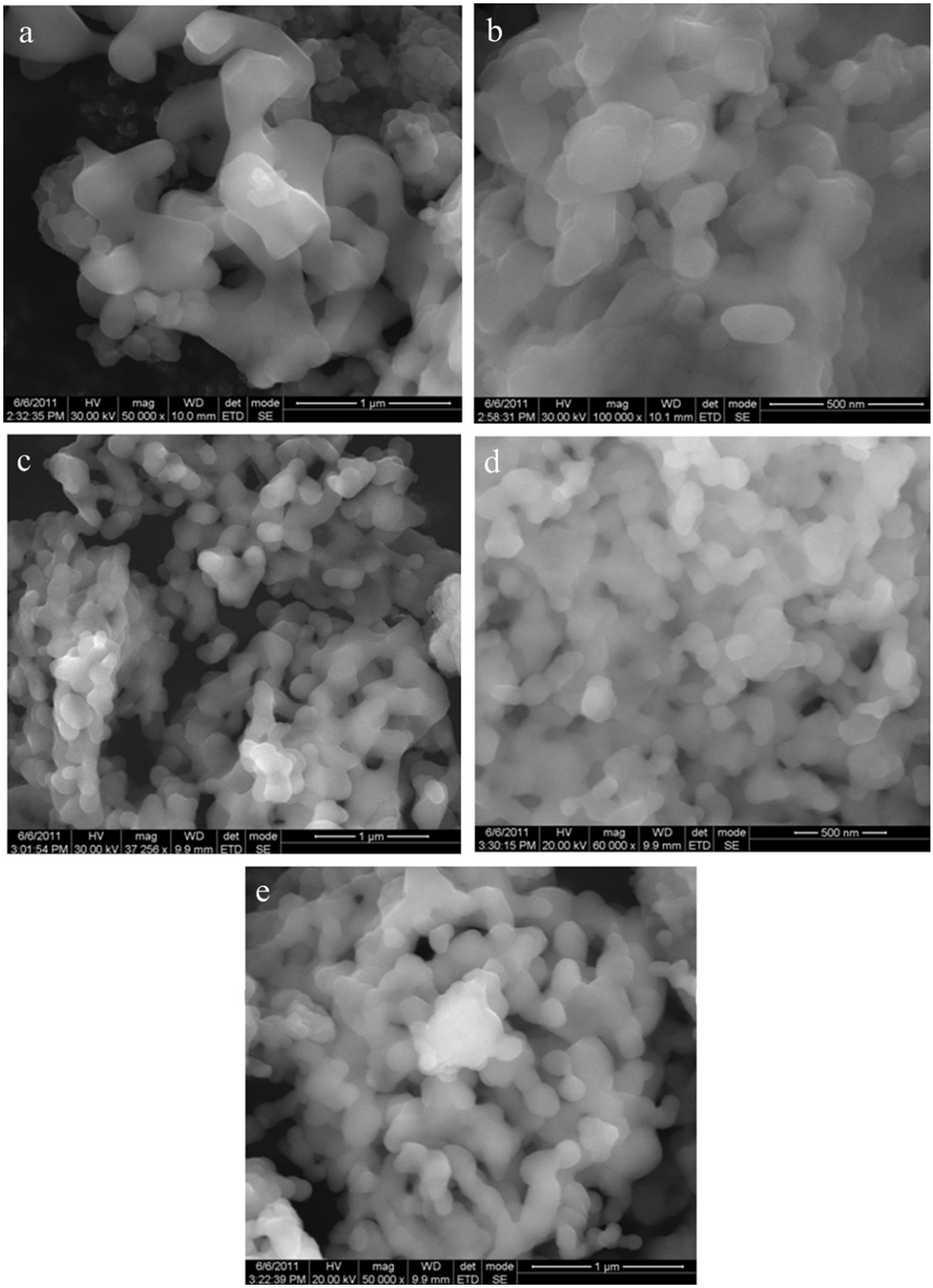

Fig. 9. SEM Micrographs of hydroxyapatites synthesized by alcohol mediated sol–gel combustion method using (a) glycine (b) alanine (c) urea (d) hydrazine (e) hexamine as fuels.

567 cm^{-1} bands arise from the components of triply degenerate v_4 OPO bending mode of PO_4^{3-} and the 472 cm^{-1} arise due to the doubly degenerate v_2 OPO bending mode of PO_4^{3-} [52,53].

The less intense bands in the 2077 $cm^{-1}$and 2003 cm^{-1} region arise due to overtones and combination of the v_3 and v_1 PO_4^{3-} modes. The well resolved bands at about 1416 cm^{-1} and 1451 cm^{-1} in the spectra are attributed to

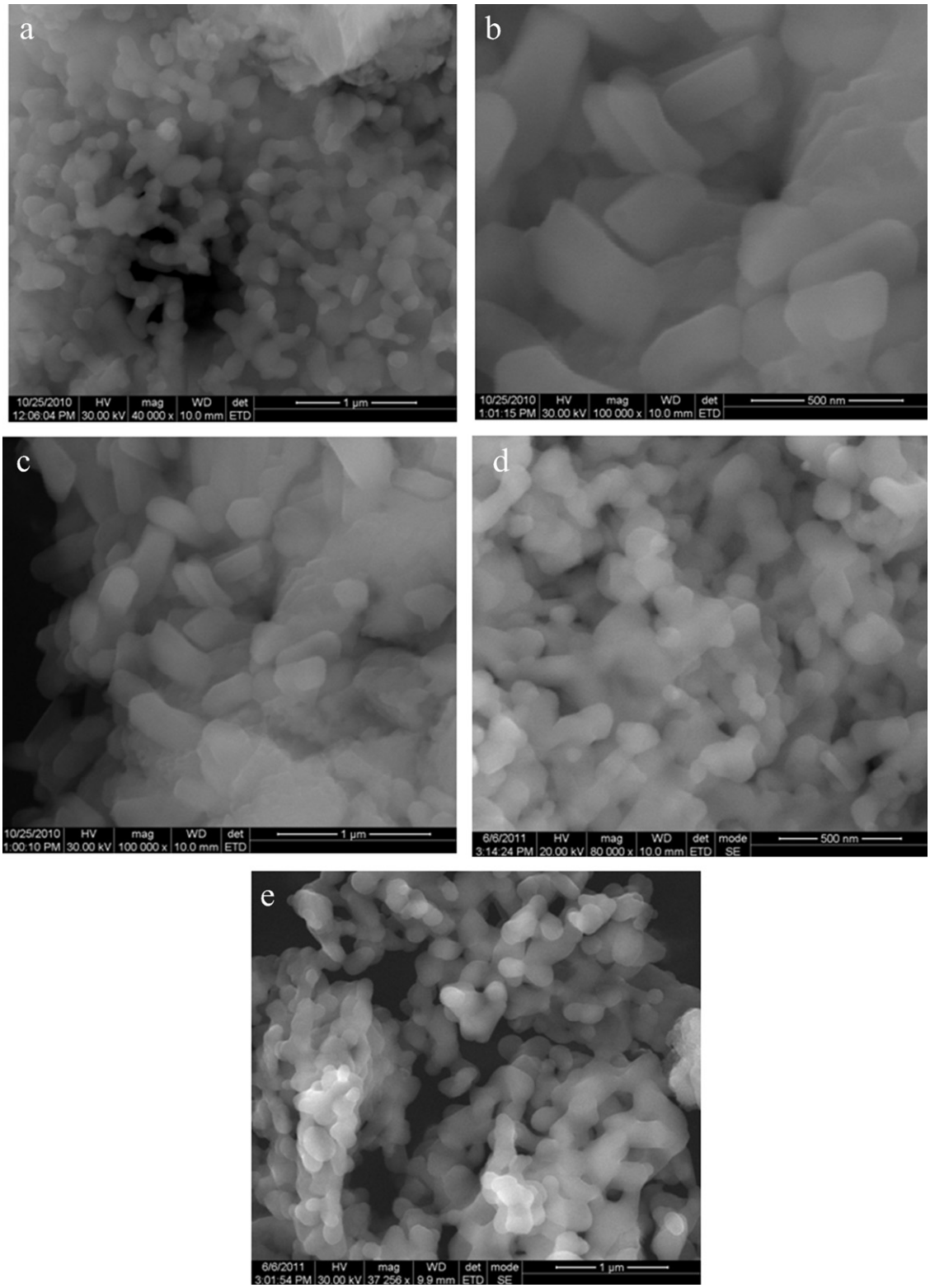

Fig. 10. SEM Micrographs of hydroxyapatites synthesized by aqueous phase sol–gel combustion method using (a) glycine (b) alanine (c) urea (d) hydrazine (e) hexamine as fuels.

the v_1 mode of CO_3^{2-}. The less intense peak at 878 cm^{-1}, assigned to the B-type of carbonate substitution, as its intensity is obscured by the HPO_4^{2-} bands in the same region. The bands at 1419 cm^{-1} and 1458 cm^{-1} correspond to v_1 mode of CO_3^{2-} which may be designated as "B-type carbonate" that replaces PO_4^{3-} ion in the hydroxyapatite lattice. The weak band at 1541 cm^{-1} corresponds to the A-type of carbonate substitution, suggesting that some of the OH ions in the hydroxyapatite lattice were replaced by carbonate ions and is comparatively less [54].

As the calcination temperature is increased to 800 °C, the crystallinity of the sample also increases. This is evident in Figs. 7 and 8 from the appearance of bands with enhanced sharpness and resolution. The peaks around 3200 cm^{-1} to 3700 cm^{-1} and 1600 cm^{-1} to 1700 cm^{-1}, have become less intense for the calcined samples, confirming that the loss was mainly due to the desorption of irreversibly adsorbed water molecules on to the surface of the ultrafine pores of the hydroxyapatite solid [55]. The fact that the peak intensity at 3572 cm^{-1} and 632 cm^{-1} has been increased after calcination, suggests the augmented crystallinity of hydroxyapatite material with the temperature. The 472 cm^{-1} band, which arises from v_2 PO_4^{3-} has been found to be exhibited by all the samples. Hydroxyapatite samples synthesized through the aqueous mediated route using fuels such as glycine, alanine and urea contains tri-calcium phosphate (TCP) as a secondary phase in addition to hydroxyapatite. The formation of biphasic mixture can be confirmed from the appearance of a broad peak around 970 cm^{-1} along with the complementary evidence from the X-ray diffraction patterns. The band at 1416 cm^{-1} and 1451 cm^{-1} which corresponds to the v_1 mode of CO_3^{2-}, becomes less intense on increasing the calcination temperature. The fact that even the samples synthesized using glycine, alanine and urea under the aqueous and alcohol combustion method contains CO_3^{2-} bands, even after the calcination at 800 °C. This indicates the strong replacement of PO_4^{3-} by CO_3^{2-} in the hydroxyapatite lattice. The calcined samples of hydroxyapatite prepared through the organic mediated combustion method exhibit well resolved and sharper peaks corresponding to PO_4^{3-} in comparison with those prepared through the aqueous mediated route.

3.3. Scanning electron microscopic analysis

The morphological images obtained using the HR-SEM analysis for the hydroxyapatites synthesised through aqueous and alcholic mediated routes calcined at 800 °C for 10 h are shown in the Figs. 9 and 10. The HR-SEM images show the presence of hydroxyapatite particles, having a cylinderical morphology and non-uniform particle sizes ranging from 30–200 nm. However, a flake like morphology was clearly visible in the case of hydroxyapatite particles prepared by the aqueous mediated route using glycine and urea as fuels. Further, the HR-SEM images also displays the presence of the agglomeration of particles in the sample prepared via both aqueous and alcohol mediated routes.

3.4. Transmission electron microscopic analysis

Hydroxyapatite samples prepared using urea as a fuel, and calcined at 800 °C were chosen for HR-TEM analysis, owing to the phase purity and a quite good morphological properties based on the XRD and HR-SEM results. Figs. 11 and 12 display the HR-TEM, SAED images and EDS profiles of hydroxyapatite synthesized through alcohol mediated combustion method using urea as fuel. The images exhibit the formation of hydroxyapatite particles with non-uniform size distribution. The bright field (BF) image of the aggregates has flake shape with a minimum size of 50 nm and a maximum of 150 nm, and the morphology corresponds to that obtained from the HR-SEM results. The selected area diffraction (SAED) pattern shows spots and ring patterns indicating the

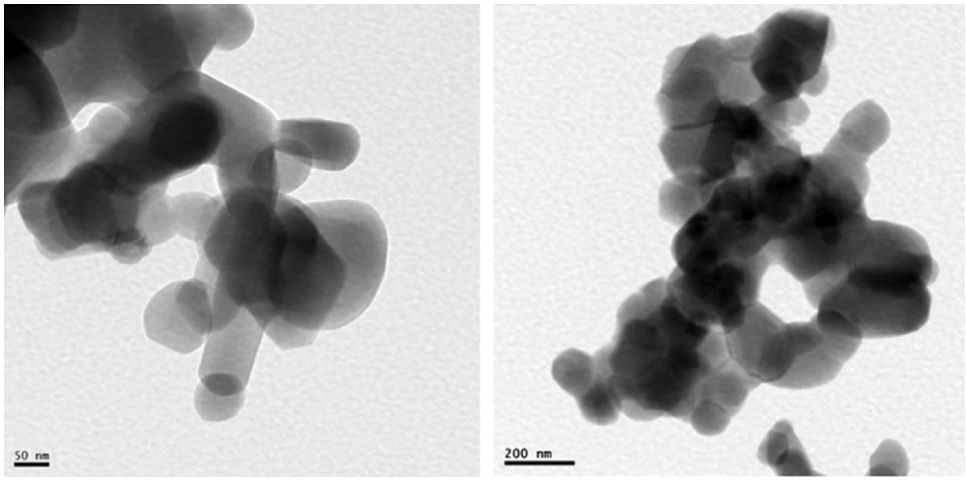

Fig. 11. TEM Micrographs of hydroxyapatite synthesized by alcohol mediated sol–gel combustion method using urea as fuel.

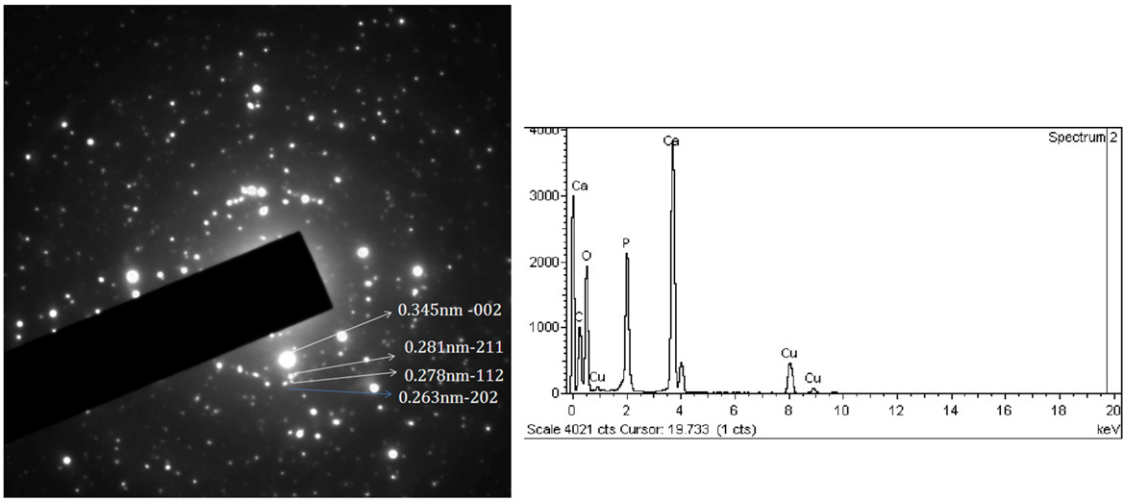

Fig. 12. (a)Selected area electron diffraction studies (SAED) and (b) EDS of hydroxyapatite synthesized by alcohol mediated sol–gel combustion method using urea as fuel.

polycrystalline nature of the hydroxyapatite, however it also shows the random orientation due to the agglomeration of platelets. Strong reflection at $d_{002}=0.345$ nm, $d_{211}=0.281$ nm, $d_{112}=0.278$ nm and $d_{202}=0.263$ nm are clearly visible in the diffraction patterns. The Ca/P ratio of 1.6 obtained from the EDS analysis is comparable with the theoretical values of Ca/P = 1.67.

4. Discussion

The aqueous mediated precipitation for the formation of hydroxyapatite using $Ca(NO_3)_2\cdot 4H_2O$ and $(NH_4)_2HPO_4$ as precursors can be represented using a stoichiometric equation as:

$$10\ Ca(NO_3)_2\cdot 4H_2O + 6(NH_4)_2HPO_4 + 8\ NH_4OH \rightarrow Ca_{10}(PO_4)_6(OH)_2 + 6H_2O + 20NH_4NO_3$$

During the precipitation process, the formation of hydroxyapatite normally proceeds under alkaline conditions above pH >11, and the predominant species stabilized under this condition will be the triply charged anion PO_4^{3-}[3,56]. The formed precipitates would be dissolved using Conc. HNO_3 and the concentrated solution was mixed then with the corresponding fuel to subject them to combustion under acidic conditions.

The aqueous based combustion can be represented using the stoichiometric equation as follows:

$$10\ Ca(NO_3)_2\cdot 4H_2O + 6(NH_4)_2HPO_4 + 11.1\ NH_2CH_2COOH + 8O_2 \rightarrow Ca_{10}(PO_4)_6(OH)_2 + 21.55\ N_2 + 93.5\ H_2O + 22.2\ CO_2$$

$$10\ Ca(NO_3)_2\cdot 4H_2O + 6(NH_4)_2HPO_4 + 10\ CH_3CH(NH_2)COOH + 22O_2 \rightarrow Ca_{10}(PO_4)_6(OH)_2 + 21N_2 + 101\ H_2O + 30CO_2$$

$$10\ Ca(NO_3)_2\cdot 4H_2O + 6(NH_4)_2HPO_4 + 16.67\ NH_2CONH_2 + 8O_2 \rightarrow Ca_{10}(PO_4)_6(OH)_2 + 32.67\ N_2 + 99.34\ H_2O + 16.67\ CO_2$$

$$10\ Ca(NO_3)_2\cdot 4H_2O + 6(NH_4)_2HPO_4 + 25\ NH_2\cdot NH_2\cdot H_2O + 8O_2 \rightarrow Ca_{10}(PO_4)_6(OH)_2 + 41\ N_2 + 141\ H_2O$$

$$10\ Ca(NO_3)_2\cdot 4H_2O + 6(NH_4)_2HPO_4 + 0.417\ C_6H_{12}N_4 + 14.25O_2 \rightarrow Ca_{10}(PO_4)_6(OH)_2 + 16.834N_2 + 68.502\ H_2O + 5.004\ CO_2$$

The carbon or coke formation during the combustion process is predictable, and the same further leads to the formation of amorphous hydroxyapatite. Additional heating treatment through calcination of the above samples would enhance the crystallinity of the hydroxyapatite phase.

In case of ethanol-mediated combustion process, the sol formed was concentrated under 110 °C while the pH was adjusted to acidic conditions. Subsequently, it was followed by the addition of given fuel resulting in the formation of the sol, which was then subjected to combustion. Hydrazine and hexamine are soluble in ethanol, which makes them homogeneous throughout the reaction medium and facilitate the combustion completely. As glycine, alanine and urea are slightly soluble in ethanol, a trace amount of water was added to dissolve the fuel prior to its dissolution in ethanol, which resulted in homogeneous reaction medium facilitating complete combustion.

The ethanol based process for the preparation of hydroxyapatite in general is expected to precede in general as follows [57]:

$$P(OR)_{3-x}(OH)_x + Ca(NO_3)_{2-y}(OR)_y \rightarrow (OR)_y(NO_3)_{2-y}\text{-}Ca\text{-}O\text{-}HPO(OR)_{3-x'} + H_2O + ROH$$

The sol thus formed resulted in the formation of hydroxyapatite on subsequent combustion. The ethanol

based combustion for various fuels can be represented by the following stoichiometric equation as follows:

$$10\ Ca\ (NO_3)_2 \cdot 4H_2O + 6\ P(OCH_2CH_3)_3 + 11.1\ NH_2CH_2COOH + 27.875\ O_2 \rightarrow Ca_{10}\ (PO_4)_6(OH)_2 + 15.55\ N_2 + 111.75\ H_2O + 58.2\ CO_2$$

$$10\ Ca\ (NO_3)_2 \cdot 4H_2O + 6\ P(OCH_2CH_3)_3 + 10\ CH_3CH(NH_2)\ COOH + 101O_2 \rightarrow Ca_{10}\ (PO_4)_6\ (OH)_2 + 15N_2 + 119H_2O + 66CO_2$$

$$10\ Ca\ (NO_3)_2 \cdot 4H_2O + 6\ P(OCH_2CH_3)_3 + 16.67\ NH_2CONH_2 + 44.005O_2 \rightarrow Ca_{10}\ (PO_4)_6\ (OH)_2 + 26.67N_2 + 117.34H_2O + 52.67CO_2$$

$$10\ Ca\ (NO_3)_2 \cdot 4H_2O + 6\ P(OCH_2CH_3)_3 + 25\ NH_2 \cdot NH_2 \cdot H_2O + 57O_2 \rightarrow Ca_{10}\ (PO_4)_6(OH)_2 + 35\ N_2 + 159\ H_2O + 36\ CO_2$$

$$10\ Ca\ (NO_3)_2 \cdot 4H_2O + 6\ P(OCH_2CH_3)_3 + 0.417\ C_6H_{12}N_4 + 35.753O_2 \rightarrow Ca_{10}\ (PO_4)_6(OH)_2 + 10.834N_2 + 86.502\ H_2O + 38.502\ CO_2$$

However, the TCP formation in ethanol mediated combustion is comparatively less ($\leq$ 0.3% of TCP/HAP) when compared to aqueous mediated combustion process($\geq$ 47% of TCP/HAP) using alanine as fuel.

It can be inferred that the lattice parameters 'a' (nm), 'c' (nm), and volume $(A^{\circ})^3$ as computed from the XRD analysis remains the same, irrespective of the medium and fuel used. However, the ratio of HAP/TCP varies with the nature of fuel and medium used for the combustion process. The lattice parameter computed from the XRD data for the hydroxyapatite material synthesised through sol–gel method and calcined at 800 °C for 10 h for the purpose of reference has shown that a = 0.9420 nm, c = 0.6866 nm and $V = 527(A^{\circ})^3$. This observation is consistent with the standard JCPDF card number 09–0432. In addition, it can be comprehended that the lattice parameters of the samples synthesized by the combustion route using alcohol medium are comparable with those of the samples prepared through the sol–gel method. The above fact establishes that the hydroxyapatites derived from the alcohol mediated combustion route are on par with those of the sol–gel derived samples.

The X-ray diffraction patterns of hydroxyapatites synthesized through alcohol mediated combustion (Fig. 8 and Table 3) has been compared with the report on the sol–gel method adopted elsewhere by Dean-Mo Liu et. al [57]. The results indicate the superiority of the current strategy in producing phase pure hydroxyapatite particles, with a relatively lesser average particle size (less than 50 nm) than reported [57].

Further, it is a known fact that hydroxyapatite generally decomposes to form CaO and TCP at higher calcination temperatures [3,58], according to the following scheme:

$$Ca_{10}\ (PO_4)_6(OH)_2 \rightarrow 2\beta\ Ca_3\ (PO_4)_2 + Ca_4O\ (PO_4)_2 + H_2O$$

$$Ca_{10}\ (PO_4)_6(OH)_2 \rightarrow 2\beta\ Ca_3\ (PO_4)_2 + CaO + H_2O$$

Dean-Mo Liu et. al., further shows the formation of β- TCP at 800 °C, whereas such decomposition is completely absent in the present investigation at 800 °C. The above fact can be confirmed by the absence of independent peaks corresponding to CaO peaks $2\theta = 37.347$ and $2\theta = 53.856$ with reference to the standard JCPDF Card no. 04–0777. Thus, the alcohol mediated combustion strategy adopted under the given conditions could be considered to be offer thermal stability to the hydroxyapatite samples.

The average crystallite size calculated from the XRD patterns and the approximate crystallite size calculated from HR-SEM analysis are given in Table 5. It can be inferred from the table that the particle sizes of hydroxyapatites prepared by all the five organic fuels have an average crystallite size much lesser than (around 50 nm) that measured using the SEM analysis. This suggests that in general, the agglomeration of particles cannot be excluded in all the samples. It is a well known fact that the particle size calculated through the XRD corresponds to average individual particles. Hence the particle size of about 50 nm obtained through the XRD could be considered in preference to that obtained through the HR-SEM in the present investigation. Moreover, HR-TEM images of urea further confirm the flake like morphology already established through the HR-SEM image.

In general, Conc. HNO_3 is known for dissolving the gel and to maintain the acidic condition throughout the reaction medium facilitating the combustion processes. However, in the present study it can be inferred that addition of Conc. HNO_3 is also found to serve as an excess oxidizer for the combustion process, thereby reducing the carbon formation in the combusted product.

It can also be inferred that the nature of fuels plays an important role in controlling the stoichiometric of the hydroxyapatite formed. The fact that the hydroxyapatite synthesized using hydrazine and hexamine as fuels has produced relatively less amount of TCP, when compared with the other fuels due to the relatively lower decomposition temperature as shown in Table 5. Hydrazine hydrate as a fuel decomposes easily to form nitrogen or ammonia, hydrogen and water at lower temperature. Hexamine having high molecular weight and high energy density of about 30.57 mJ/kg; added to the combustion process as a fuel, burns smokeless leading to combustion without carbonaceous residues [59]. The Table 5 further indicates that the decomposition temperature of glycine and alanine are higher than the urea, hydrazine and hexamine and hence therefore the latter fuels can be considered to facilitate the combustion at higher temperatures.

In an aqueous medium the relative binding strength of amino acids as organic fuel such as glycine, alanine towards calcium may also lead to the formation of monomeric, dimeric and trimeric complexes at the time of combustion [60]. Since the relative binding strength of alanine with Ca^{2+} is higher than that of glycine, the latter facilitates the decomposition reaction of calcium deficient apatite leading

Table 5
Heat of combustion, decomposition temperature and energy density for five organic fuels used for combustion synthesis of hydroxyapatites.

Fuel	Glycine	Alanine	Urea	Hydrazine hydrate	Hexamine
Molecular weight (g/mol)	80.1	90.1	60.1	50.06	140.2
Heat of combustion (kJ/mol)	−974.1	−1621	−634.1	−613	−4288
Decomposition temperature (C)	814	260	153	135	175
Energy density (mJ/Kg)	12.16	17.99	10.55	12.25	30.57

towards the formation of TCP. The above fact could very well be justified by the %HAP/TCP ratio of 53/47 for alanine and 64/36 for glycine as can be referred from the Table-1. Urea reacts with $Ca(NO_3)_2 \cdot 4H_2O$ to form an adduct, $Ca(NO_3)_2 \cdot 4[N_2H_4CO]$, thus facilitating the combustion process of the non-stoichiometric apatite in addition to the stoichiometric hydroxyapatite. It can be reasonably speculated that addition of nitric acid to dissolve the sol, with the subsequent addition of organic fuels such as glycine, alanine and urea would have caused the binding of fuel with calcium in the aqueous medium. Consequently, combustion could have led into the formation of biphasic mixtures.

However, in case of the alcohol mediated combustion process, the addition of a trace amount of water to hydrolyze the triethyl phosphite does not have much bearing on the hydroxyapatite formation, irrespective of the fuel added. The mechanism for the formation of alcohol based hydroxyapatite formation could be explained, based on the equations given below [61]:

$$Ca(NO_3)_2 \cdot 4H_2O + C_2H_5OH \rightarrow Ca(NO_3)_2(OC_2H_5)_x + H_2O$$

$$P(OCH_2CH_3)_3 + H_2O \rightarrow HPO(OCH_2CH_3)_3 + C_2H_5OH$$

$$HPO(OCH_2CH_3)_3 + H_2O \rightarrow HPO(OCH_2CH_3)_{2\text{-}x}(OH)_x + xC_2H_5OH$$

$$2HPO(OCH_2CH_3)_{2-x}(OH)_x + Ca(NO_3)_2(OC_2H_5)_x \rightarrow Ca[OPO(OCH_2CH_3)_{2-x}(OH)_x]_2 + 2H^+$$

Triethyl phosphite undergoes hydrolysis on the addition of a trace amount of water and the hydrolyzed phosphite interacts with the calcium ions to form calcium phosphate intermediate through a condensation polymerization reaction. This calcium phosphate intermediate was then made acidic by adding conc. HNO_3, which would completely hydrolyze the triethyl phosphite to form ethanol as solvent and the combustion would have facilitated the stoichiometric hydroxyapatite formation thereby generating a stable and phase pure hydroxyapatite.

5. Conclusion

The proposed method of producing hydroxyapatite bioceramics conserves time and energy, involves a simple and easy procedure, in comparison with the existing wet and dry chemical methods. This investigation leading, to the comparison of various fuels in two different media, is the first of its kind in the existing literature reports, and could pave the way for broader knowledge about this system. On comparing both the aqueous and alcohol mediated combustion processes, the latter proves to be a promising route to produce phase pure hydroxyapatite. Among the five organic fuels employed, the hydrazine based aqueous mediated combustion process yielded nearly a phase purity of 90%. The rest of the five organic fuels have been found to be ideal for the organic mediated route, producing phase pure hydroxyapatite, with the formation of a negligible amount of TCP $\leq 0.3\%$. In addition, to the best of our knowledge, the current strategy is the first of its kind in reporting the synthesis of hydroxyapatite in acidic environment through an alcohol mediated combustion method, resulting in phase pure hydroxyapatite, with a relatively smaller average particle size(less than 50 nm) than reported throughout the literature. Moreover, the present strategy holds the advantage of both the ethanol based sol–gel and combustion methods, and further possesses the potential to be scaled up to synthesize phase pure and nano-sized hydroxyapatite.

References

[1] H. Aoki, Science and medical applications of hydroxyapatite, Japanese Association of Apatite Science, Tokyo, Japan, 1991.
[2] W. Suchanek, M. Yoshimura, Processing and properties of hydroxyapatite-based biomaterials for use as hard tissue replacement implants, Journal of Materials Research 13 (1998) 94–117.
[3] J.C. Elliot, Structural and chemistry of the apatites and other calcium orthophosphates, Elsevier, Amsterdam, 1994.
[4] T. Matsumoto, M. Okazaki, M. Inoue, S. Yamaguchi, T. Kusunose, T. Toyonaga, Y. Hamada, J. Takahashi, Hydroxyapatite particles as a controlled release carrier of protein, Biomaterials 25 (2004) 3807–3812.
[5] Feng Ye, Haifeng Guo, Haijiao Zhang, Xiulan He, Polymeric micelle-templated synthesis of hydroxyapatite hollow nanoparticles for a drug delivery system, Acta Biomaterialia 6 (2010) 2212–2218.
[6] Yung Chin Yang, Edward Chang, Measurements of residual stresses in plasma-sprayed hydroxyapatite coatings on titanium alloy, Surface and Coatings Technology 190 (2005) 122–131.
[7] Min Wang, Developing bioactive composite materials for tissue replacement, Biomaterials 24 (2003) 2133–2151.
[8] K.C.B. Yeong, J. Wang, S.C. N, Mechanochemical synthesis of nanocrystalline hydroxyapatite from CaO and $CaHPO_4$, Biomaterials 22 (2001) 2705–2712.
[9] J. Arends, J. Christoffersen, M.R. Christoffersen, H. Eckert, B.O. Fowler, J.C. Heughebaert, G.H. Nancollas, J.P. Yesinowski, S.J. Zawacki, A calcium hydroxyapatite precipitated from an aqueous solution: an international multimethod analysis, Journal of Crystal Growth 84 (1987) 515–532.

[10] M. Akao, H. Aoki, K. Kato, Mechanical properties of sintered hydroxyapatite for prosthetic applications, Journal of Materials Science 16 (1981) 809–812.
[11] Wei Menghan Ma, Xiao-Xiang Ye, Wang, Effect of supersaturation on the morphology of hydroxyapatite crystals deposited by electrochemical deposition on titanium, Materials Letters 62 (2008) 3875–3877.
[12] D.M. Liu, T. Troczynski, W.J.T. Seng, Aging effect on the phase evolution of water-based sol–gel hydroxyapatite, Biomaterials 23 (2002) 1227–1236.
[13] Ming-Fa Hsieh, Li-Hsiang Perng, Tsung-Shune Chin, Huann-Guang Perng, Phase purity of sol–gel-derived hydroxyapatite ceramic, Biomaterials 22 (2001) 2601–2607.
[14] H.S. Liu, T.S. Chin, L.S. Lai, S.Y. Chiu, K.H. Chung, C.S. Chang, M.T. Liu, Hydroxyapatite synthesized by a simplified hydrothermal method, Ceramics International 23 (1997) 19–25.
[15] Yadong Li Yan, Zhao-Xiang Li, Jin Deng, Zhuang, Xiaoming Sun, Surfactant-assisted hydrothermal synthesis of hydroxyapatite nanorods, International Journal of Inorganic Materials 3 (2001) 633–637.
[16] George C. Koumoulidis, Alexandros P. Katsoulidis, Athanasios K. Ladavos, Phillippos J. Pomonis, Christos C. Trapalis, Antonios T. Sdoukos, Tiberius C. Vaimakis, Preparation of hydroxyapatite via microemulsion route, Journal of colloid and Interface Science 259 (2003) 254–260.
[17] E. Iyyappan, P. Wilson, Synthesis of nanoscale hydroxyapatite particles using triton X-100 as an organic modifier, Ceramics International (2012).
[18] K.C. Patil, M.S. Hegde, Tanu Rattan, S.T. Aruna, Chemistry of nanocrystalline oxide materials: combustion synthesis, properties and applications, World Scientific, Singapore, 2008.
[19] K.C. Patil, S.T. Aruna, S. Ekambaram, Combustion synthesis, Current Opinion in Solid State and Materials Science 2 (1997) 158–165.
[20] K.C. Patil, S.T. Aruna, T. Mimani, Combustion synthesis: an update, Current Opinion in Solid State and Materials Science 6 (2002) 507–512.
[21] Xiaoming Guo, Dongsen Mao, Guanzhong Lu, Song Wang, Guisheng Wu, Glycine–nitrate combustion synthesis of CuO–ZnO–ZrO_2 catalysts for methanol synthesis from CO_2 hydrogenation, Journal of Catalysis 271 (2010) 178–185.
[22] Lei Shi, Kai Tao, Ruiqin Yang, Fanzhi Meng, Chuang Xing, Noritatsu Tsubaki, Study on the preparation of Cu/ZnO catalyst by sol–gel auto-combustion method and its application for low-temperature methanol synthesis, Applied Catalysis, A: General 401 (2011) 46–55.
[23] X. Zhu, T. Zhang, D. Marchant, V. Morris, Combustion synthesis of TiC–NiAl composite by induction heating, Journal of the European Ceramic Society 30 (2010) 2781–2790.
[24] S. Ekambaram, K.C. Patil, M. Maaza, Synthesis of lamp phosphors: facile combustion approach, Journal of Alloys and Compounds 393 (2005) 81–92.
[25] Vijay Singh, T.K.Gundu Rao, Jun-Jie Zhu, Preparation, luminescence and defect studies of Eu^{2+}-activated strontium hexa-aluminate phosphor prepared via combustion method, Journal of Solid State Chemistry 179 (2006) 2589–2594.
[26] Tomohiro Akiyama, Hiromichi Isogai, Jun-ichiro Yagi, Reaction rate of combustion synthesis of an intermetallic compound, Powder Technology 95 (1998) 175–181.
[27] Singanahally T. Aruna, Alexander S. Mukasyan, Combustion synthesis and nanomaterials, Current Opinion in Solid State and Materials Science 12 (2008) 44–50.
[28] E. Chinarro, J.R. Jurado, M.T. Colomer, Synthesis of ceria-based electrolyte nanometric powders by urea-combustion technique, Journal of the European Ceramic Society 27 (2007) 3619–3623.
[29] Xun Tianyou Peng, Ke Liu, Jiangrong Dai, Haibo Xiao, Song, Effect of acidity on the glycine–nitrate combustion synthesis of nanocrystalline alumina powder, Materials Research Bulletin 41 (2006) 1638–1645.
[30] Satish Samantaray, B.G. Mishra, D.K. Pradhan, G. Hota, Solution combustion synthesis and physicochemical characterization of ZrO_2–MoO_3 nanocomposite oxides prepared using different fuels, Ceramics International 37 (2011) 3101–3108.
[31] M. Edriss M, R. Norouzbeigi, Synthesis and characterization of alumina nanopowders by combustion of nitrate–amino acid gels, Polymers and Materials Science 25 (2007) 1029–1040.
[32] Jianjun Ma, Cairong Jiang, Xiaoliang Zhou, Guangyao Meng, Xingqin Liu, A facile combustion synthesis of Ce0.8Sm0.2O1.9 powders by in situ assembly of polymer, Journal of Alloys and Compounds 455 (2008) 364–368.
[33] S. Vivekanandhan, M. Venkateswarulu, N. Satyanarayana, Ammonium carboxylates assisted combustion process for the synthesis of nanocrystalline $LiCoO_2$ powders, Materials Chemistry and Physics 109 (2008) 241–248.
[34] Ying chao Han, Shipu Li, Xinyu Wang, Xiaoming Chen, Synthesis and sintering of nanocrystalline hydroxyapatite powders by citric acid sol–gel combustion method, Materials Research Bulletin 39 (2004) 25–32.
[35] V.B. Taxak, S.P. Khatkar, Sang-Do Han, Rajesh Kumar, Mukesh Kuma, Tartaric acid-assisted sol–gel synthesis of Y2O3:Eu3+ nanoparticles, Journal of Alloys and Compounds 469 (2009) 224–228.
[36] M.M. Rashad, S.M. El-Sheikh, Magnetic properties of nano-clusters lanthanum chromite powders doped with samarium and strontium ions synthesized via a novel combustion method, Materials Research Bulletin 46 (2011) 469–477.
[37] Rekha Kiranmala Laishram, Neelam Mann, Malhan, Single step synthesis of yttrium aluminum garnet ($Y_3Al_5O_{12}$) nanopowders by mixed fuel solution combustion approach, Ceramics International 37 (2011) 3743–3746.
[38] R. Jimenez, X. Garcia, T. Lopez, A.L. Gordon, Catalytic combustion of soot. Effects of added alkali metals on CaO–MgO physical mixtures, Fuel Processing Technology 89 (2008) 1160–1168.
[39] Nguyen Vu, Tran Kim Anh, Gyu-Chul Yi, W. Strek, Photoluminescence and cathodoluminescence properties of Y_2O_3:Eu nanophosphors prepared by combustion synthesis, Journal of Luminescence 122-123 (2007) 776–779.
[40] L.C. Nehru, V. Swaminathan, C. Sanjeeviraja, Rapid synthesis of nanocrystalline ZnO by a microwave-assisted combustion method, Powder Technology 226 (2012) 29–33.
[41] S.R. Jain, K.C. Adiga, V.R.Pai Verneker, A new approach to thermochemical calculations of condensed fuel-oxidizer mixtures, Combustion and Flame 40 (1981) 71–79.
[42] H.K. Varma, S.N. Kalkurab, R. Sivakumar, Polymeric precursor route for the preparation of calcium phosphate compounds, Ceramics International 24 (1998) 467–470.
[43] A. Cuneyt Tas, Combustion synthesis of calcium phosphate bioceramic powders, Journal of the European Ceramic Society 20 (2000) 2389–2394.
[44] Yingchao Han, Shipu Li, Xinyu Wang, Xiaoming Chen, Synthesis and sintering of nanocrystalline hydroxyapatite powders by citric acid sol–gel combustion method, Materials Research Bulletin 39 (2004) 25–32.
[45] Samir K. Ghosh, Samit K. Nandi, Biswanath Kundu, Someswar Datta, K.De Dipak, Sujit K. Roy, Debabrata Basu, In vivo response of porous hydroxyapatite and β-tricalcium phosphate prepared by aqueous solution combustion method and comparison with bioglass scaffolds, Journal of Biomedical Materials Research, Part B: Applied Biomaterials 86B (2007) 217–227.
[46] Yuan Yuan, Changsheng Liu, Yuan Zhang, Xiaoqian Shan, Sol–gel auto-combustion synthesis of hydroxyapatite nanotubes array in porous alumina template, Materials Chemistry and Physics 112 (2008) 275–280.
[47] Yoshio Waseda, Eiichiro Matsubara, Kozo Shinoda, X-Ray diffraction crystallography, Springer, 2011.
[48] E. Caroline Victoria, F.D. Gnanam, Synthesis of calcium phosphates and porous hydroxyapatite beads prepared by emulsion method, Trends in Biomaterials and Artificial Organs 16 (2002) 12–14.

[49] Bing-Hung Chen, Kang-I Chen, Mei-Ling Ho, Hong-Nian Chen, Wen-Cheng Chen, Chih-Kuang Wang, Synthesis of calcium phosphates and porous hydroxyapatite beads prepared by emulsion method, Materials Chemistry and Physics 113 (2009) 365–371.
[50] E. Landi, A. Tampieri, G. Celotti, S. Spiro, Densification behaviour and mechanisms of synthetic hydroxyapatites, Journal of the European Ceramic Society 20 (2000) 2377–2387.
[51] M.I. Kay, R.A. Young, A.S. Posner, Crystal Structure of Hydroxyapatite, Nature 204 (1964) 1050–1052.
[52] B.O. Fowler, Infrared studies of apatites. I. Vibrational assignments for calcium, strontium, and barium hydroxyapatites utilizing isotopic substitution, Inorganic Chemistry 13 (1) (1974) 194–207 1.
[53] B.O. Fowler, Infrared studies of apatites. II. Preparation of normal and isotopically substituted calcium, strontium, and barium hydroxyapatites and spectra-structure-composition correlations, Inorganic Chemistry 13 (2) (1974) 207–214.
[54] J.C. Elliot, D.W. Holcomb, R.A. Young, Infrared determination of the degree of substitution of hydroxyl by carbonate ions in human dental enamel, Calcified tissue international 37 (1985) 372–375.
[55] Helga Füredi-Milhofer, V. Hlady, Frederick S Baker, Ralph A Beebe, Nancy Wolejko Wikholm, J.S. Kittelberger, Temperature-programmed dehydration of hydroxyapatite, Journal of Colloid and Interface Science 70 (1979) 1–9.
[56] Mathai Mathew, Shozo Takagi, Structures of Biological Minerals in Dental Research, Journal of research of the National Institute of Standards and Technology 106 (2001) 1035–1044.
[57] Dean-Mo Liu, T. Troczynski, Wenjea J. Tseng, Water-based sol–gel synthesis of hydroxyapatite: process development, Biomaterials 22 (2001) 1721–1730.
[58] S. Raynaud, E. Champion, D. Bernache-Assollant, P. Thomas, Calcium phosphate apatites with variable Ca/P atomic ratio I. Synthesis, characterisation and thermal stability of powders, Biomaterials 23 (2002) 1065–1072.
[59] M.T. Carayon, J.L. Lacout, Study of the Ca/P atomic ratio of the amorphous phase in plasma-sprayed hydroxyapatite coatings, Journal of Solid State Chemistry 172 (2003) 339–350.
[60] Yen-Peng Ho, Ming-Wei Yang, Li-Ting Chen, Yu-Chuan Yang, Relative calcium-binding strengths of amino acids determined using the kinetic method, Rapid Communications in Mass Spectrometry 21 (2007) 1083–1089.
[61] D.M. Liu, T. Troczynski, D. Hakimi, Effect of hydrolysis on the phase evolution of water-based sol–gel hydroxyapatite and its application to bioactive coatings, Journal of Materials Science: Materials in Medicine 13 (2002) 657–665.